

FILE COPY

Final Technical Report on FY90 SORP
1990

D-A229 902

Randall S. Jacobson
ONR Code 1125GG

My FY90 SORP, "Attenuation of compressional waves in oceanic crust", has been fruitful. The proposal was to analyze a high quality seismic refraction data set to obtain compressional wave attenuation models for oceanic crust. The specific tasks and results are:

Complete the attenuation analysis and publish the results. Despite the late delivery of the computer to do the analysis, I was able to finish the work and write a manuscript (R. S. Jacobson and B. T. R. Lewis, The First Direct Measurements of Compressional Wave Attenuation in the Uppermost Oceanic Crust). This paper has been published in the Journal of Geophysical Research (v. 95, B11, pp. 17,417-17,429) and is attached. The basic conclusions of this work were:

- (a) Values of Q (a measure of the attenuation) cluster between 20 and 50, an order of magnitude greater attenuation than estimated by forward modeling by others.
- (b) Variability of the results strongly implicate heterogeneities within the crust on scales of 100's of meters.
- (c) The attenuation estimates are considered normal to high, based upon the use of the sonar equation to match signal to noise ratios as a function of frequency of historical data.
- (d) Values of Q around 50 are sufficient to limit propagation of seismic energy within the crust to be below 20 Hz for typical seismic refraction profiles.

Additional work was directed towards joint inversion of travel time and amplitude data for velocity-depth information. I have written software to correct all the seismic data for input into the inversion program. The development of the software for the inversion, testing of the inversion methodology, and the analysis of the results has been completed. The results were somewhat disappointing, perhaps due to errors in location of the shot positions in three dimensions. A further test of this methodology is expected in the future by inversion of another data set, using electrically detonated explosive shots, providing accurate origin times of the source. Other progress relates to the unexpected task of determining the rank of matrices for inversion. A completely objective method has been found to determine which eigenvalues are non-zero using Chi-square analysis and Fisher Tests. This combination of error analysis and statistical analysis has yet to be applied to inversion theory but is often used for other types of problems. I have instituted a literature search for applications, theoretical developments, etc. A software package has been developed to use this methodology, and I am currently using it in inversion applications.

DTIC
ELECTE
DEC 11 1990
S D

DISTRIBUTION STATEMENT A
Approved for public release
Distribution Unlimited

Accession For	
NHS	CRA&I ✓
DTIC	TAB
Unannounced	
Justification	
By	
Distribution /	
Availability	
Dist	Avail and/or Special
A-1	



90 1 124

Statement "A" per telecon Dr. Randall Jacobson. Office of Naval Research/ code 1125GG.

VHG

12/10/90

The First Direct Measurements of Upper Oceanic Crustal Compressional Wave Attenuation

R. S. JACOBSON

Office of Naval Research, Arlington, Virginia

B. T. R. LEWIS

School of Oceanography, University of Washington, Seattle, Washington

The first direct measurement of compressional wave attenuation of the uppermost 650 m of oceanic crust was performed using data recorded by seafloor hydrophones and large (56-116 kg), deep, explosive sources. The site was 13 km east of the southernmost Juan de Fuca Ridge on crust 0.4 m.y. old. Spectral ratios were performed between bottom refracting waves and direct water waves, adjusted for spreading losses and transmission coefficient losses. Several tests of the data were performed, demonstrating that attenuation is linearly related to frequency between 15 and 140 Hz, but frequency-independent components of attenuation are also evident. Values of compressional wave Q cluster between 20 and 50 and do not show any systematic variation with depth over 650 m. The attenuation results also indicate the presence of heterogeneities within the crust, as the solutions for each receiver's data set are significantly different. No evidence for azimuthal variations of attenuation are supported by the data, although the data do not optimally sample a wide variation of azimuths. Our attenuation values are judged to be normal to higher than expected for the whole oceanic crust, based upon comparisons to results from synthetic seismogram modeling by others and by modeling signal to noise ratios of typical seismic refraction profiles. The results are consistent with recent laboratory measurements at ultrasonic frequencies for dry and saturated basalts at seafloor pressures and temperatures.

INTRODUCTION

Despite decades of investigations of the oceanic crust and mantle using seismic refraction techniques, knowledge of the velocity and attenuation structure of the uppermost kilometer is the most deficient [Spudich and Orcutt, 1980a]. Despite the fact that seismic energy must propagate through this portion of the crust to be received by either on-bottom, midwater or near-surface sensors, nature appears to conspire against investigations of this most accessible portion of oceanic lithosphere. To isolate the effects of the uppermost crust upon seismic wave propagation requires a concomitant isolation of other interfering energy paths. To optimize this effort, both sources and receivers should be near the seafloor, so that interfering water-borne energy will arrive at times sufficiently distinct from those paths traveling within the bottom. Two decades of refraction experiments using surface charges and ocean bottom seismometers have revealed little of the detailed nature of the uppermost kilometer of crust, although some gross averages can be obtained [Ewing and Purdy, 1982]. Recent multichannel studies with high spatial resolution [e.g., Harding *et al.*, 1989; Vera, 1989] have revealed details of the uppermost velocity structures and seafloor velocities. Vertical or oblique seismic profiling has also proved effective for determining upper crustal velocities [e.g., Stephen *et al.*, 1980; Stephen and Harding, 1983; Little and Stephen, 1985]. Only recently have experimental techniques been tried to use near-bottom charges for seismic refraction profiling [e.g., Jacobson *et al.*, 1981; Purdy, 1986; Sauter *et al.*, 1986], with success. There are several disadvantages using deep explosive charges, including higher frequency content, more complicated logistics, more time required to perform the experiment, and increased safety concerns. The goal of obtaining more detailed seismic information of seismic layer 2 is closer to being achieved,

particularly in concert with results from drilling the oceanic crust by the Deep Sea Drilling Project and the Ocean Drilling Project.

The seismic results to date are entirely in terms of compressional wave velocity structures, often showing steep gradients with depth that are a function of crustal age [Purdy, 1987]. Other information regarding seismic structures, such as compressional wave attenuation, shear velocity, and attenuation structures, are either unavailable for analysis in existing data sets or have not been investigated. These additional seismic structures can be useful not only for further resolving the geologic stratigraphy but are also crucial to understanding the full impact of upper oceanic crustal structures on seismic wave propagation into and out of the oceanic lithosphere.

In 1985, we conducted a deep source, deep receiver seismic refraction experiment on 0.4 m.y. old crust 13 km east of the southernmost Juan de Fuca Ridge (Figure 1). The site was chosen to coincide with a previous experiment that used a deep-towed seismic streamer and air guns along a profile shot parallel to the spreading direction [Lewis and Jung, 1984]. Analysis of those data demonstrated that the frequency dependence of attenuation was essentially independent of observational range or depth of penetration. Further analysis by Lewis and Jung [1989] found that P wave Q between 10 and 50 for the upper 1 km at this site were consistent with the data. They also suggested the possibility of velocity structures within the bottom that create "resonances" due to ducting of seismic energy that are frequency dependent and modify any attenuation that may occur. The experimental geometry of the deep-towed streamer data set was suboptimal to determine the fine structure of attenuation parameters with depth.

EXPERIMENTAL CONFIGURATION AND DESIGN

To test the hypothesis for the anomalous attenuation due to velocity "resonances" required an unusual experimental configuration. The goals were to determine simultaneously the compressional wave velocity and attenuation structure with depth and to examine the azimuthal dependence of attenuation.

Deep explosive charges were needed with sufficient energy and

Copyright 1990 by the American Geophysical Union.

Paper number 90JB00808.
0148-0227/90/90JB-00808\$05.00

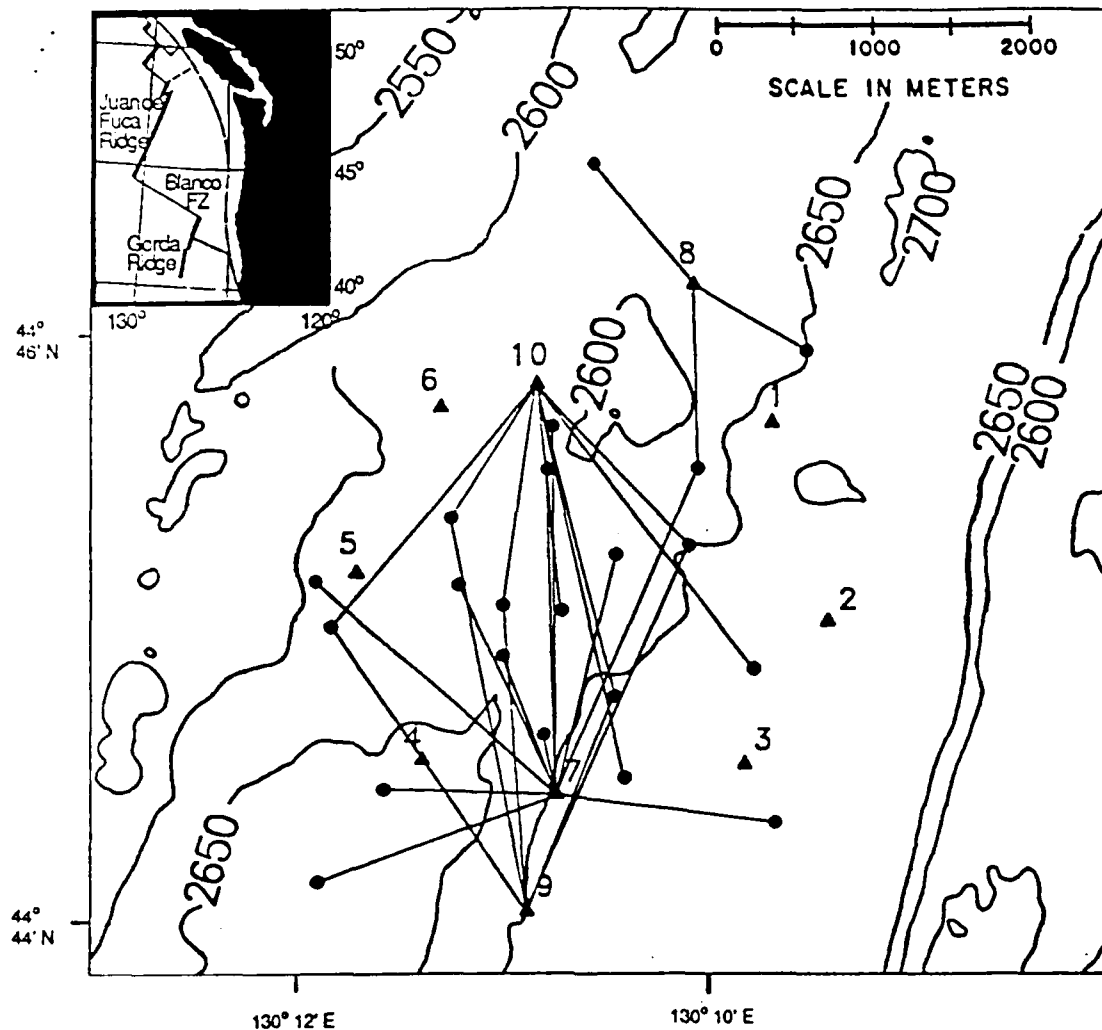


Fig. 1. A map derived from Sea Beam bathymetry of the experimental site located 13 km east of the southernmost Juan de Fuca Ridge. The solid triangles indicate the locations of the ocean bottom seismometers (1-6) and the seafloor hydrophones (7-10); only the SFH data were used to invert for attenuation. The solid dots are the shot locations, and the interconnecting lines indicate the shot-receiver combinations used in the analysis. The ray paths are heavily biased to the north and south, a result of experimental geometry and possibly propagation effects. The contours are in uncorrected meters.

bandwidth to overcome the high attenuation expected. TNT and C4 plastic explosives were detonated by (SUS) Sound Underwater Source [Naval Ordnance System Command, 1973] MK 59 devices, set to 1829 or 2438 nominal meters (6000 or 8000 feet). Charge sizes ranged from 58 to 116 kg, yielding maximum energies at 50-60 Hz. Bottom charges, designed to excite shear waves, consisted of approximately 3 kg of explosives in a "pipe bomb". These charges were largely unsuccessful, as the energy needed to release the end cap was insufficient to overcome ambient hydrostatic pressures.

Receivers consisted of digitally recording seafloor hydrophones [Shor, 1979], with 126 dB of dynamic range, 66 dB of resolution, and 200 Hz effective bandwidth with 1-ms sampling. Due to power limitations, two hydrophone systems were deployed twice; on the second deployment, one of the seafloor hydrophones (SFH9) was deployed approximately 700 m above the bottom, so that uncontaminated source signatures could be recorded. In addition, six triaxial ocean bottom seismometers were deployed, which recorded analog seismic signals on magnetic tape, yielding a bandwidth of approximately 100 Hz and a dynamic range of 80 dB after decompression [Johnson et al., 1977]. The ocean bottom seismometer data were not analyzed in this paper due to the limited bandwidth of the instruments.

All of the instruments were deployed in a 3-km-diameter array in an area of flat seafloor, 2600 m deep, 13 km east of the Juan de Fuca Ridge (Figure 1). Box and gravity cores recovered up to 0.39 m of fine dark brown silt over heavy grey clay. Shipboard and bottom pingers were unable to resolve sediment thickness, which is thought to be no more than a couple of meters thick. At the seismic frequencies of interest (≤ 150 Hz), the sedimentary cover should have an insignificant impact upon experimental results.

Navigation consisted of LORAN C and transit satellites, both generally accurate to 100 m when available. Bathymetry consisted of 3.5- and 12-kHz-wide beam echo sounders and Sea Beam coverage of the area was provided by NOAA.

Two separate sequences of shots were deployed in a star pattern to permit varying azimuths and ranges to the receivers. Corrections to the hydrophone refraction data were reported by Poujol and Jacobson [1988]. All shots were corrected to the entry point at the seafloor, defined by the Sea Beam bathymetry using the water path correction of Purdy [1982]. A record section was plotted (Figure 2), and travel times were picked manually. The resultant travel time plot is shown in Figure 3 with a third-order polynomial fit, which was later used to facilitate the determination of the velocity depth function [Poujol and Jacobson, 1988].

ATTENUATION

To determine the attenuation parameters from seismic refraction data, one needs to account for all mechanisms that can modify the amplitude and frequency content of the propagating wave. The received signal, $A(x, \omega)$, is affected by spreading losses, reflection, and/or transmission losses, instrumental response, and attenuation:

$$A(x, \omega) = A_0(0, \omega) e^{i\alpha x} e^{-\alpha(\omega)x} \frac{R(x, \omega)}{G(x)} I(\omega) \quad (1)$$

where x is the distance, ω is the angular frequency, $A_0(0, \omega)$ is the source function, $\exp[-\alpha(\omega)x]$ is the attenuation due to propagation, $R(x, \omega)$ is the total loss due to reflections and transmissions, $G(x)$ represents the spreading loss, and $I(\omega)$ is the instrument transfer function. The direct water wave path can be expressed as

$$A_w(x, \omega) = A_0(0, \omega) e^{i\alpha x} e^{-\alpha_w(\omega)x} \frac{I(\omega)}{G_w(x)} \quad (2)$$

where $\exp[-\alpha_w x]$ is the attenuation through the water (hereafter α_w is assumed to be zero), and subscript w represents the direct water wave. Dividing equation (1) by equation (2) and taking logarithms, we obtain

$$\ln \left[\frac{A(x, \omega)}{A_w(x, \omega)} \right] = -\alpha(\omega)x + \ln R(x, \omega) + \ln \left[\frac{G_w(x)}{G(x)} \right] \quad (3)$$

We will assume that there are no caustics and that all frequency dependence is in α ; that is, both $R(x, \omega)$ and spreading losses are independent of frequency. The term αx can be rewritten several ways [e.g. Johnston and Toksöz, 1981], including

$$\alpha(\omega)x = \pi F x Q^{-1}(F) V^{-1}(F) = \pi F T(F) Q^{-1}(F) \quad (4)$$

where T is the travel time through the attenuating medium and F is the frequency in hertz. Equation (4) allows for velocity dispersion and a frequency-dependent quality factor Q . In general, although

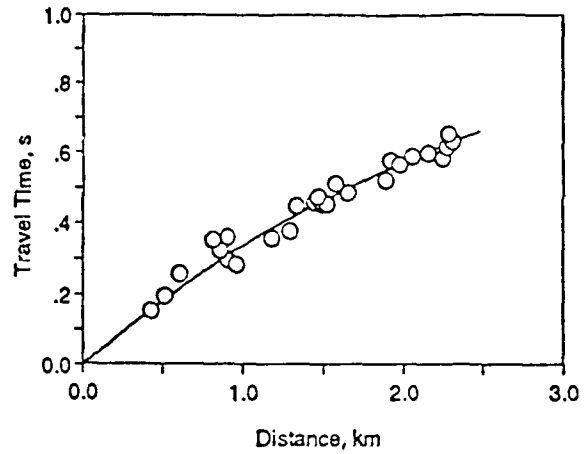


Fig. 3. Seafloor hydrophone travel time data (circles) used for the inversion of the velocity depth function, which in turn is used to constrain the spreading losses. A third-order polynomial fit to the data is also shown.

Q can also vary with depth, we will assume for the moment that $Q(F)$ is constant throughout the bottom. Given these assumptions and definitions, equation (3) can be rewritten as

$$\ln \left[\frac{A(x, F)}{A_w(x, F)} \right] = -\pi F T(F) Q^{-1}(F) + \ln R(x) + \ln \left[\frac{G_w(x)}{G(x)} \right] \quad (5)$$

Considering only those terms that are frequency dependent and further assuming that $T(F)$ is independent of frequency, the specific quality factor Q^{-1} can be found to be

$$Q^{-1}(F) = \frac{1}{\pi F T} \left[\ln \left(\frac{A_w(x, F)}{A(x, F)} \right) \right] \quad (6a)$$

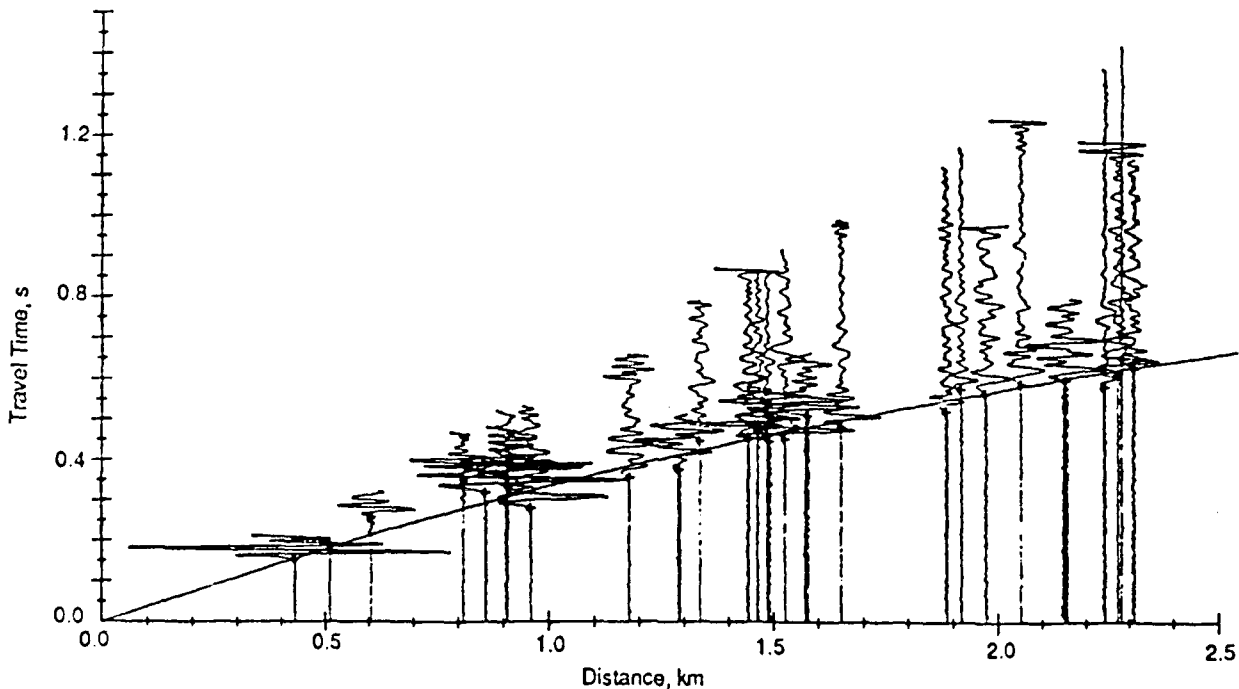


Fig. 2. True amplitude, unreduced, record section of the seafloor hydrophone data with the predicted travel time curve, based upon a third-order polynomial. The traces were terminated at the water wave arrival and equalized for shot size variations by $W^{A/B}$, where W is the weight in pounds. No clear evidence of converted shear waves is present in the data. The chaotic nature of the intertrace coherence is due to the widely varying shot depths, which affects both the frequency content of the source function and the amplitudes, due to spreading losses.

If the logarithm of the spectral ratio is assumed or found to be linearly dependent upon frequency and if one assumes that the frequency-independent terms of equation (5) do not affect Q^{-1} in any way, then

$$Q^{-1} = \frac{1}{\pi F} \frac{\partial}{\partial F} \left[\ln \left(\frac{A_w(x, F)}{A(x, F)} \right) \right] \quad (6b)$$

where Q^{-1} is now independent of frequency. The assumptions of frequency-independent Q^{-1} , T , and a linear dependence of the logarithm of the spectral ratio with frequency violate the principles of causality [cf. *Kjartansson*, 1979 and *Jacobson*, 1987]. Equation (6b), although physically unrealizable, is often used as the spectral ratio method for seismic refraction profiles [e.g., *Jacobson et al.*, 1981, 1984]. Equation (6a) is the more appropriate relationship to investigate attenuation, despite the fact that *Jacobson* [1987] demonstrated that velocity dispersion, $V(F)$, or equivalently $T(F)$, as well as frequency-dependent Q can be measured using seismic refraction methodologies. Frequency dependence of the attenuation coefficient can be tested simply, using the form

$$\alpha(F) = \pi F^m T Q^{-1} \quad (7)$$

lumping the frequency dependence of T and Q^{-1} into the power of frequency dependence, m . Attenuation due to scattering can also exhibit frequency-independent components, so that a better test may be

$$\alpha(F) = \pi F^m T Q_0^{-1} + B \quad (8)$$

where B is a term independent of frequency. *Jacobson* [1987] expanded this definition to

$$\alpha(F) = \pi F T \left(Q_0^{-1} F^a + \frac{A_1}{F} + \frac{A_2}{T} \right) - A_3 \quad (9)$$

to search for a more complete, empirical, description of the effects of scattering attenuation. To do so requires the calculation of the $R(x)$ and $G(x)$ terms, which can be misconstrued as frequency-independent components of attenuation.

The spreading loss term, $G(x)$, for a flat earth can be derived from the equation for a spherically symmetric earth [*Aki and Richards*, 1980, p. 120]:

$$G(x) = \frac{1}{V_s} \left[\cos(\theta_r) \cos(\theta_s) \frac{x}{p} \left(\frac{\partial x}{\partial p} \right) \right]^{1/2} \quad (10)$$

where p is the slowness, θ refers to the angle of the ray with respect to the vertical and subscripts r and s refer to the receiver and source, respectively. The term $\partial x / \partial p$ equal to $(\partial^2 t / \partial x^2)^{-1}$ can be obtained from the travel time curve or by manipulation of the velocity depth function to yield $x(p)$. In a layered media, x must be replaced by Σx and $\partial x / \partial p$ by $\Sigma \partial x / \partial p$ over the layers the wave propagates.

The reflection and transmission coefficients can be calculated from equations given by *Aki and Richards* [1980], if one knows or assumes the compressional and shear wave velocities and densities throughout the entire structure of interest. Further assumptions include planar waves, smooth boundaries, and no velocity gradients, all of which can modify the reflection and transmission coefficients. The appropriate coefficients can only be predicted with reasonable accuracy at the seafloor interface. Since the details of the subbottom structure are unknown, we are forced to incorporate subbottom losses due to transmissions and reflections into the attenuation coefficients.

Equation (9) can be used to examine the data for frequency-dependent quality factors, Q^{-1} , as well as frequency-independent terms that indicate a "DC" shift in attenuation. *Jacobson* [1987] has interpreted these terms to indicate either a frequency dependence of

Q below the lowest frequency measured or offsets of attenuation due to interbed multiples or to scattering from heterogeneities.

Provided the data indicate no frequency dependence of Q within the measured bandwidth and relaxing the assumption of a depth independent Q , we can solve for $Q(z)$. To do so requires knowledge of the ray path geometry for each shot, easily obtained by ray tracing, knowing the velocity depth function. This method allows a direct mapping of total travel time T or total subbottom distance x into an equivalent bottoming depth z where the ray turns horizontal [cf. *Dorman and Jacobson*, 1981]. Keeping the frequency-independent terms, the more general form of equation (5) becomes

$$\ln \left[\frac{A(x, F)}{A_w(x, F)} \right] = -\pi F T Q^{-1}(z) + \ln R(x) + \ln \left[\frac{G_w(x)}{G(x)} \right] \quad (11)$$

Assuming an attenuation model consisting of a series of layers, each with a constant Q^{-1} , and retaining the discretized frequency, F_i , equation (11) can be rewritten as

$$\ln \left[\frac{A_j(x, F_i)}{A_{w_j}(x, F_i)} \right] = \sum_{k=1}^m (-\pi F_i T_{jk} Q_k^{-1}) + \ln R_j(x) + \ln \left[\frac{G_{w_j}(x)}{G_j(x)} \right] \quad (12)$$

where subscript j denotes a particular shot-receiver pair and subscript k denotes the layer number. T_{jk} represents the travel time of the j th ray in layer k ; similarly, Q_k^{-1} is the contribution of attenuation to the spectral ratio for layer k , equal to

$$Q_k^{-1} = Q_{0k}^{-1} + \frac{B'_k}{F_i} \quad (13)$$

where B' describes the frequency-independent components of attenuation α analogous to equation (8).

Once the effects of attenuation are isolated from all other parameters, the azimuthal dependence of attenuation can be determined. An empirical test of azimuthal dependence of attenuation can be performed via

$$Q^{-1}(z, \varphi) = Q_0^{-1}(z) \sum a_i \cos(\varphi_i) + b_i \sin(\varphi_i) \quad (14)$$

Only even powers of a and b should exist, as the presence of odd powers would violate reciprocity.

VELOCITY RESULTS

To analyze properly the data for attenuation as a function of depth it is necessary to determine the velocity depth function. *Poujol and Jacobson* [1988] reported on the velocity inversion for the seafloor hydrophone data only, using the τ - ξ inversion of *Dorman and Jacobson* [1981]. Their results indicate a seafloor velocity of 2.7 km s⁻¹, with high velocity gradients, ranging from 4.6 s⁻¹ at the surface to 4.1 s⁻¹ at 679 m depth, the maximum extent of the data. The maximum velocity observed was 5.6 km s⁻¹. The velocity depth profile (Figure 4) is extremely smooth, showing no sharp velocity changes usually associated with layer 2A-B stratigraphy. This is probably not real but is simply the result of oversmoothing of the travel time curve used to invert the velocity depth function.

Poujol and Jacobson [1988] point out, however, that considerable scatter in their waveforms may be due to local crustal heterogeneities. In particular, one seafloor hydrophone (SFH8) recorded an unusual high-frequency, low-amplitude precursor on several of the records, due to what might be a local high-velocity block of crustal material. Further evidence of crustal heterogeneities can also be found in the ocean bottom seismometer data. Although a similar inversion technique for velocity structure using all available data [*Jung*, 1988] revealed similar structures to those as reported by *Poujol and Jacobson* [1988], two of the ocean

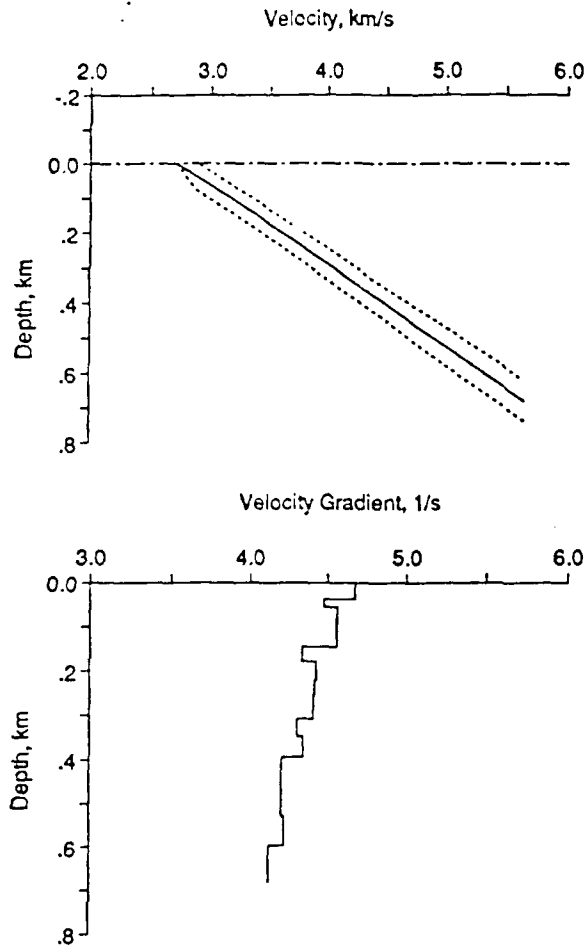


Fig. 4. The velocity depth solution with 95% error bounds and the velocity gradient solution obtained by inverting the travel time data.

bottom seismometers (OBS2 and OBS6) recorded converted shear waves. Assuming a V_p/V_s ratio of 1.8 at the seafloor, a shear wave velocity of 1.5 km s^{-1} would permit conversion to shear wave energy at the seafloor. If the shear velocity dips below the overlying water velocity, conversion to shear energy becomes increasingly inefficient. If the shear (and compressional) velocities at the seafloor vary by 0.1 km s^{-1} due to crustal inhomogeneities, significant variations of shear wave energies will result. No clear converted shear wave energy was observed on the hydrophone data (Figure 2).

For the attenuation analysis, only the seafloor hydrophone data will be used, as the ocean bottom seismometer data were too band-limited. To be internally consistent, the velocity structure determined by *Poujol and Jacobson [1988]* will be used in the subsequent analysis. The differences between the velocity structures determined by *Jung [1988]* and *Poujol and Jacobson [1988]* are minor; the effects on the attenuation results using either velocity structure are insignificant.

ATTENUATION ANALYSIS

To determine the attenuation structure versus depth, one must first calculate the spectral ratio (equation (6)). Both the refracted energy and the direct waterborne arrivals were box-car windowed into 0.064-s segments, except the most close-in arrival, which was windowed into a 0.032-s time segment. No other smoothing operations were performed on the data. Only the first refracted arrivals were used; no other refracted phases could be identified. Fast

Fourier transforms of the windowed data were performed, the spectral ratios determined, and converted into logarithms. Typical spectra (Figure 5) displayed a flattening of the spectral levels beyond 150 Hz, indicating digital noise due to limited resolution. Each spectral ratio was examined for sufficient signal to noise ratios, and only data with adequate signals were retained for further analysis.

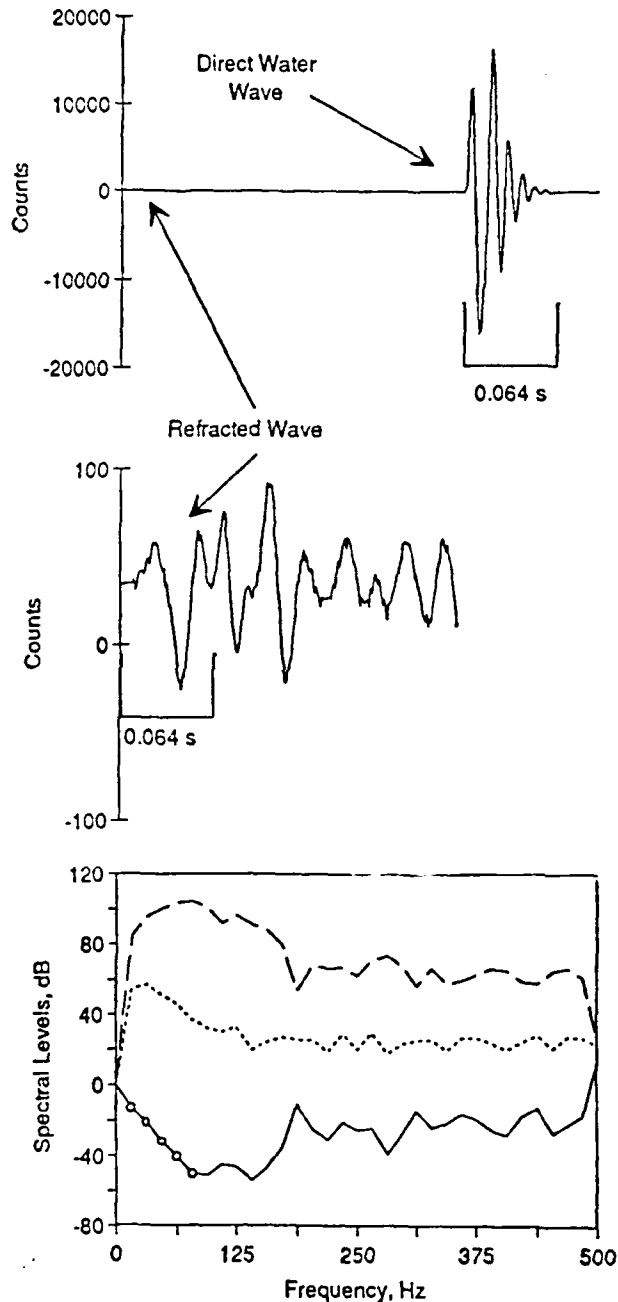


Fig. 5. (Top) A seismic trace recorded by SFH9 at a reduced distance of 2.154 km, beginning at the first refracted arrival time. The direct water wave, which dominates the trace, was windowed with a 0.064-s box-car for spectral analysis. The vertical axis is in digital counts. (Middle) The same seismic trace as above, except expanded to show only the refracted arrival. There is a small DC offset in the trace due to the gain-ranging amplifiers. The first 64 ms of data were selected for spectral analysis. (Bottom) The spectral plot of the direct water wave (large dashes), the refracted wave (small dashes) and the corrected spectral ratio (solid). The ordinate is in decibels relative to digital counts for the direct and water waves. The spectral ratio data, adjusted for spreading losses and transmission losses, are in decibels. The circles represent the data actually used for the inversion of attenuation.

Most of the data were confined to the bandwidth 15-94 Hz, although some data extended to 140 Hz. To examine the existence of frequency-independent components of attenuation, the raw spectral ratio data were adjusted for spreading losses using equation (10) and for transmission losses across the water-basement interface.

Tests for Frequency Dependence of Attenuation

The first examination of the data was to look for frequency dependence of the attenuation coefficient $\alpha(F)$ by using equation (9). Various permutations of the coefficients were examined, as the coefficients are not orthogonal. F tests were used to determine the significance of variance reductions with the addition of each new coefficient. Results of the tests indicate that the combined data set (ALL) should be broken down into individual data sets appropriate to each of the four receivers, as discussed below. In all five cases, the attenuation coefficient was found to have a linear dependence of frequency ($n=0$ of equation (9)) within the bandwidth of available data (15.625-140.625 Hz). Each data set did exhibit some time- and/or frequency-independent components of attenuation (e.g., A_1 , A_2 and A_3 of equation (9)). In three cases (SFH8, SFH10, and ALL) some frequency-independent component of attenuation was exhibited (Table 1). These coefficients can be interpreted as a non-zero intercept of a linear fit to the adjusted spectral ratio data for each shot. By calculating a slope and intercept for each shot, a qualitative fit of the models in Table 1 to the data can be seen in Figure 6. In all cases, the predicted slopes increase with bottoming depth (equivalent to subbottom travel time or range). For SFH10 and ALL, the intercepts are largely negative, increasing to slightly positive values below 550 m. Negative intercepts for this model (equation (9)) imply an excess attenuation at zero frequency, where attenuation hypothetically should be zero. Anomalous sources of attenuation (e.g., scattered or apparent attenuation) and/or incorrect adjustments (spreading losses, transmission losses) are likely explanations for the intercept offsets.

SFH7 and SFH9 models exhibit a component of spectral slope other than zero at the seafloor (Figures 6a and 6c), resulting from the time-independent component of attenuation A_2 . Since equation (9) is simply an empirical description of attenuation, it is difficult to hypothesize a source for this component of α .

All of the models have values of Q_0 between 23 and 67, much lower than those values determined by synthetic seismogram modeling [e.g., Spudich and Orcutt, 1980b]. There is little evidence of range (or depth) independent variations of the spectral slope, since most of the data clusters between -0.4 and -0.8 dB Hz⁻¹ (Figure 6). Similarly, most of the spectral intercepts of the data cluster around zero, suggesting the adjustments made to the data are largely correct. This latter observation can be construed as evidence for the lack of

caustics in the travel time data, which would otherwise produce a pronounced excess of intercept values at range or depth.

Statistical tests (e.g., Bartlett's test for homogeneity of variance [Ostle and Mensing, 1975]) indicate a significant difference in variances between the individual receiver data sets, implying the differences in these models are real. Additionally, the four in-

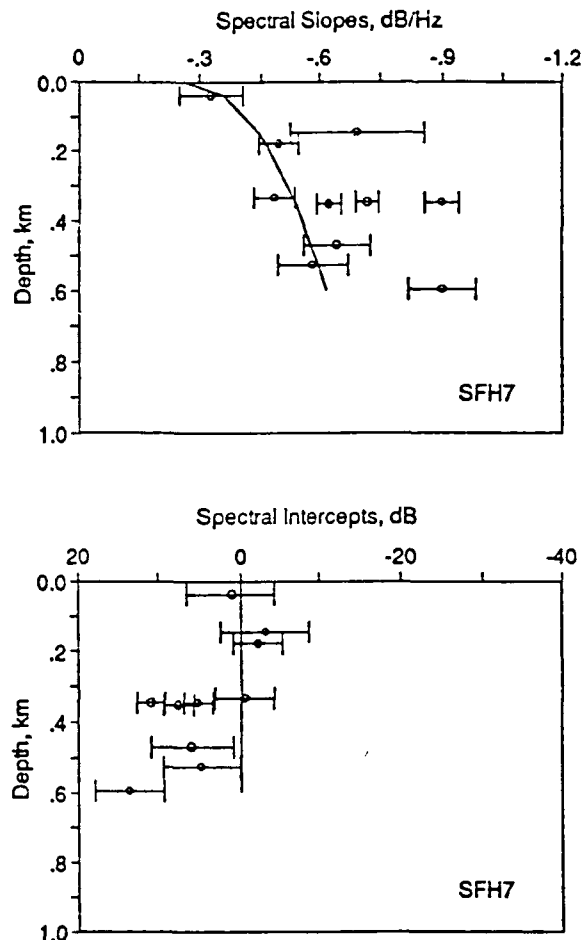


Fig. 6a. Plots of the fit of the solutions using equation (9) and Table 1 to the various data sets, after equation (9) was converted to decibels by multiplication of 8.686. (Top) The fit of the spectral slope component of equation (9) as a function of bottoming depth to a regression of each shot's spectral ratio data of SFH7 by a slope and intercept. The circles represent the best fit slope, and the error bounds correspond to a $\pm 1\sigma$ range. The inversion for attenuation uses the data at each frequency for each shot and does not attempt to fit the slope-intercept combination. (Bottom) The fit of the solution using equation (9) to the spectral intercept of SFH7 data.

TABLE 1. Model Solution of SFH Data Sets to Equation (9), Before Conversion to Decibels (Multiplicative Factor of 8.686).

	SFH7	SFH8	SFH9	SFH10	ALL
Q_0^{-1}	0.0215 (0.0052)	0.0307 (0.0067)	0.0150 (0.0174)	0.0444 (0.0052)	0.0423 (0.0025)
n	—	—	—	—	—
A_1	—	—	—	-1.4789 (0.4094)	-1.9004 (0.2244)
A_2	0.0093 (0.0022)	—	0.0147 (0.0091)	—	—
A_3	—	-3.2075 (0.4418)	—	-2.6350 (0.05617)	-3.1754 (0.02930)
Number of data	55	18	23	37	133
σ	6.61 dB	11.15 dB	5.41 dB	7.87 dB	8.73 dB

The values in parentheses are the one standard deviation values of the solution parameters. The large dashes indicate that these parameters were not statistically different from zero and therefore were not required to fit the data.

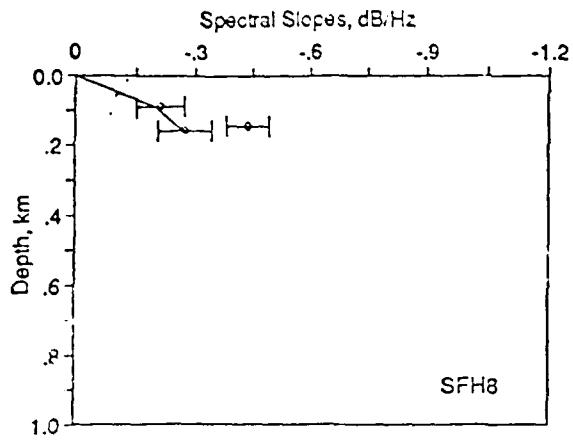


Fig. 6b. Same as Figure 6a, except using only the data from SFH8.

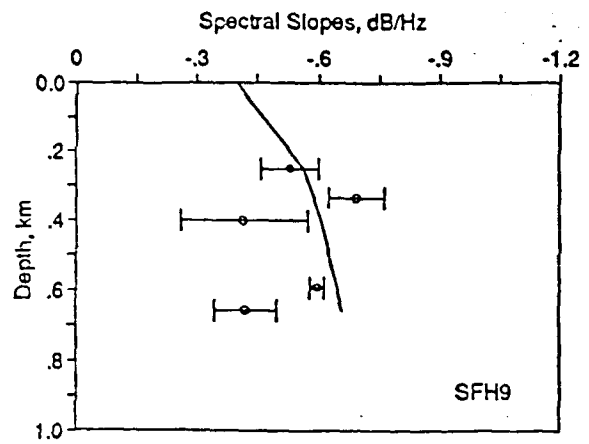


Fig. 6c. Same as Figure 6a, except using only the data from SFH9.

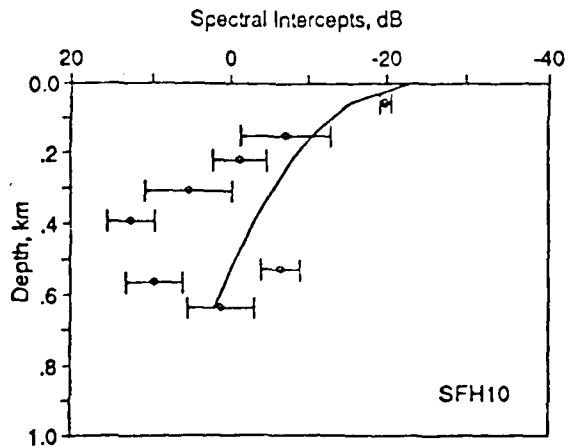
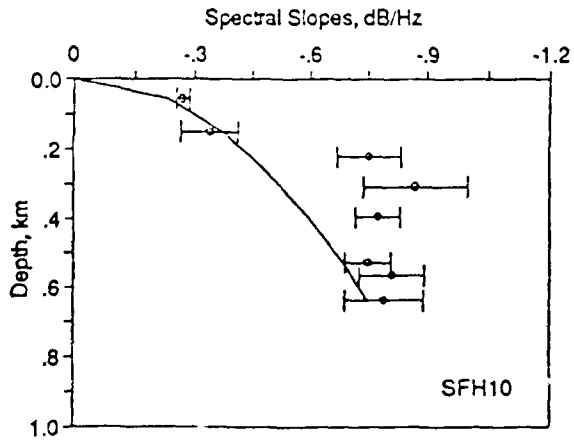
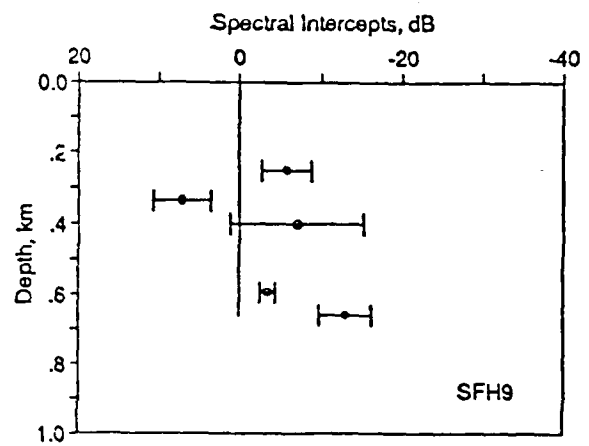
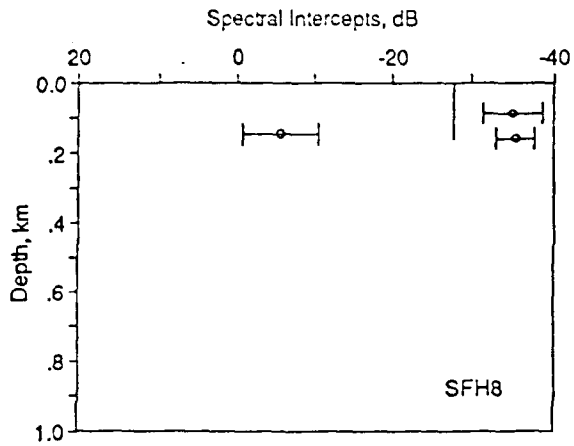


Fig. 6d. Same as Figure 6a, except using only the data from SFH10.

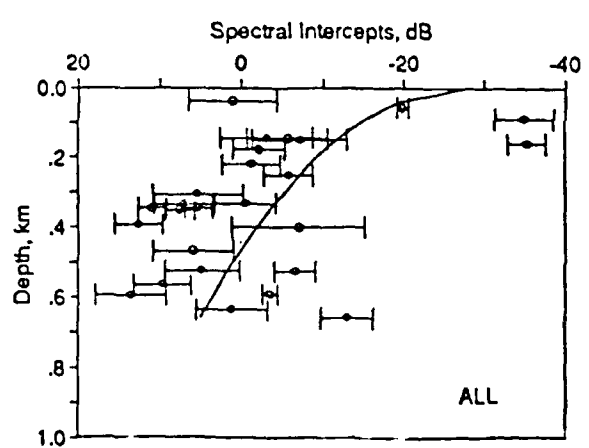
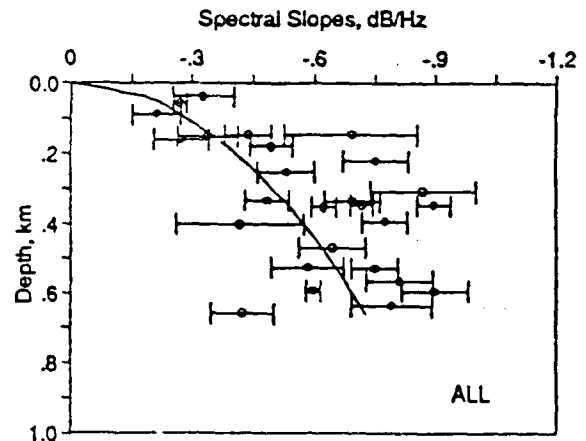


Fig. 6e. Same as Figure 6a, except using all of the data from every receiver.

dividual data sets have a combined residual variance significantly lower than the model fitting all the data simultaneously. It appears that within the 3-km array, differences of attenuation of the oceanic crust exist on this spatial scale. Similar results for spatial heterogeneities of velocity within the crust have been determined by Stephen [1988] for DSDP site 504B and by Swift and Stephen [1989] for old Atlantic crust.

Attenuation Versus Depth Results

One of the conclusions of fitting the data to equation (9) was that α varies linearly with frequency, so equations (12) and (13) can be used to examine the detailed aspects of variations of attenuation with depth. One set of models for the five data sets consisted of a single layer of attenuation. The results were quite similar to those in Table 1 and Figure 6 and thus are not shown. One difference, however, is that equations (12) and (13) force the spectral slope and the spectral intercept components to be zero at the seafloor. Only the model fitting SFH8 data required a nonzero value of the spectral intercept at depth. Values of Q_0 of all the models varied between 20 and 30, clustering around the lower value. Again, there was a significant reduction of residuals using the individual data sets relative to data set ALL, and the variances between the four individual data sets were again inhomogeneous. This emphasizes the interpretation of attenuation heterogeneities within the hydrophone array.

The next set of models were determined by maximizing the depth resolution of attenuation. Up to 14 layers, matching the layering of the velocity depth function, were allowed to be fit with a Q^{-1} and the B' parameter (equation (13)). Some of the layers contained multiple rays turning horizontally within the layer. The data consist of the corrected spectral ratio values as a function of frequency, as shown in Figure 5. A singular value decomposition routine [Wiggins, 1972] was used to search for the maximum number of eigenvalues and eigenvectors permissible with positive values of Q^{-1} . F tests were used to determine whether the reduction of variance with increasing number of eigenvalues was justified. The solutions to the five data sets are shown in Figure 7 and the fit to the data in Figure 8. The data and associated errors shown in Figure 8 are the slopes and intercepts found by linear regression for each shot's spectral ratio values and are used solely for qualitative examinations of the model fit to the data. All of the solutions, except that for SFH9, required a nonzero intercept term, typically between 15 and -15 dB s^{-1} . The values of Q_0 vary between 4 and 275 but cluster between 20 and 50. F tests again indicate that the individual models are better than the model fitting the ALL data set. Tests for homogeneity of variance indicates the variances are now homogeneous between the various receiver models, suggesting that portions of the individual solutions may have some degree of commonality. The residual standard deviations for models fitting data sets SFH7, 8, 9, 10, and ALL are 5.63, 7.07, 5.27, 4.71, and 7.77 dB, respectively. These residuals are much lower than those determined by fitting the data to equation (9), not surprising considering the increased number of parameters used to fit the data. These models, shown in Figures 7 and their fit to the data in Figure 8, are our preferred solutions to the data.

Finally, the residuals from the solutions in Figure 7 were examined for azimuthal variations using equation (14). Only SFH7 residuals had a significant reduction of variance using a 10 term for the intercept. This result is physically unreasonable, as it implies reciprocity does not hold. It can be interpreted, however, as indicating some degree of heterogeneity, since the data set (as well as all of the others) does not truly sample all azimuths and there are no reciprocal paths.

DISCUSSION

Perhaps the most intriguing result of this study was the consistently low values of Q , regardless of which model was used to fit the data. The values of the quality factor cluster tightly between 20 and 50, much lower than those determined by Jacobson *et al.* [1981, 1984] for sediments but similar to those inferred by Lewis and Jung [1989] for oceanic crust at our site. Values of Q obtained by forward modeling of synthetic seismograms [cf. Spudich and Orcutt, 1980b; Collins *et al.*, 1989] suggest values of Q closer to 500, an order of magnitude less attenuation. Vera [1989] examined multichannel data from the East Pacific Rise and found a Q of about 80 to match amplitude variations as a function of offset. Spudich and Orcutt [1980b] admit that their constraints for Q_p based upon synthetic seismograms are poor, likely the result of the trade-off of amplitudes between the velocity depth function (which alters the spreading loss) and attenuation. Further, the narrow band source functions typically used in synthetic seismogram modeling to increase computational speed and to mimic the resulting energy spectral content of the seismic refraction profiles limits the frequency resolution necessary to constrain attenuation.

Wepfer and Christensen [1987, this issue] reported the first laboratory measurements of Q for dry and water-saturated oceanic basalts under pressure and temperature conditions appropriate for

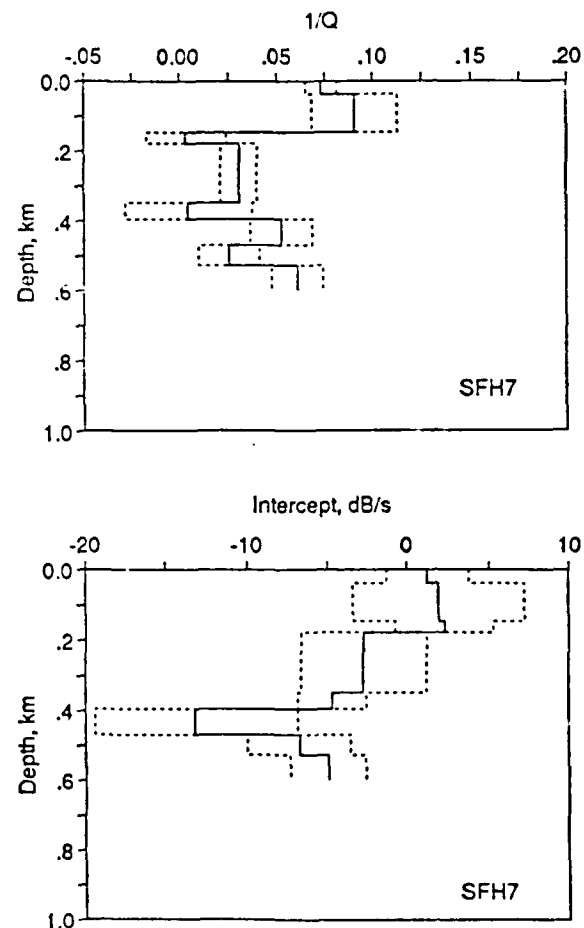


Fig. 7a. Solutions of the attenuation varying as a function of depth using equations (12) and (13), after conversion to decibels, and maximizing the depth resolution for SFH7. (Top) Plot of Q_0^{-1} as a function of depth (solid) and $\pm 1\sigma$ error bounds (dashed). (Bottom) Plot of B' , the frequency-independent component of attenuation, as a function of depth (solid) and $\pm 1\sigma$ error bounds (dashed).

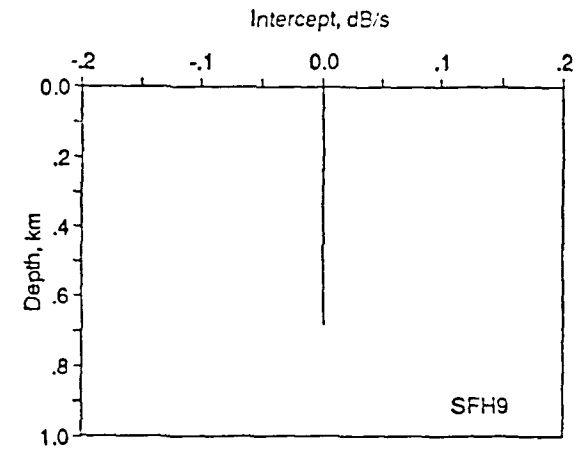
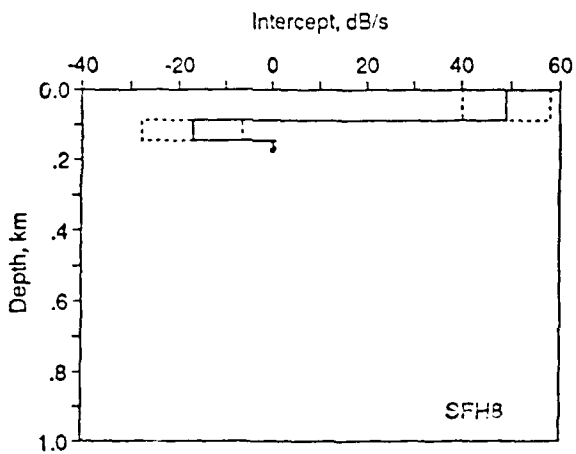
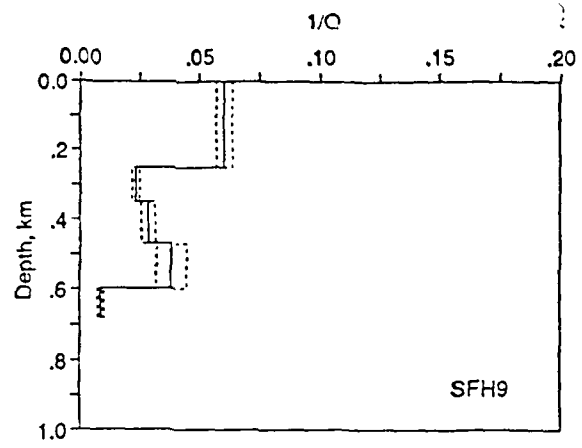
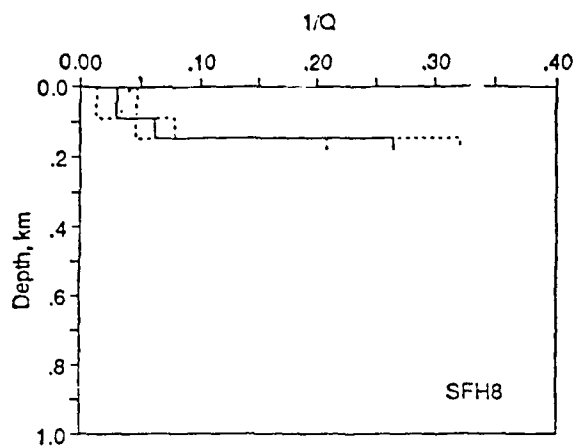


Fig. 7b. Same as Figure 7a, except using only the data from SFH8.

Fig. 7c. Same as Figure 7a, except using only the data from SFH9. The solution does not require a frequency-independent component of attenuation.

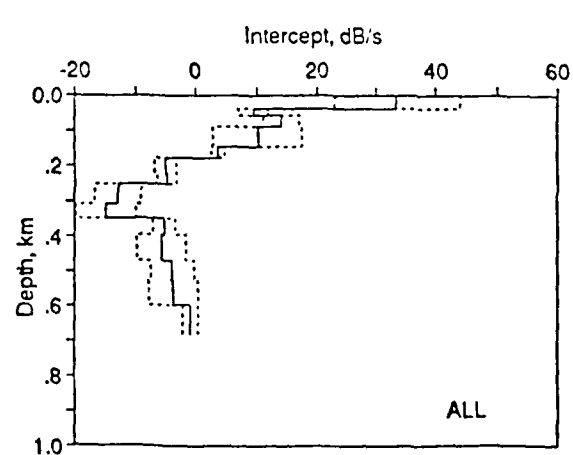
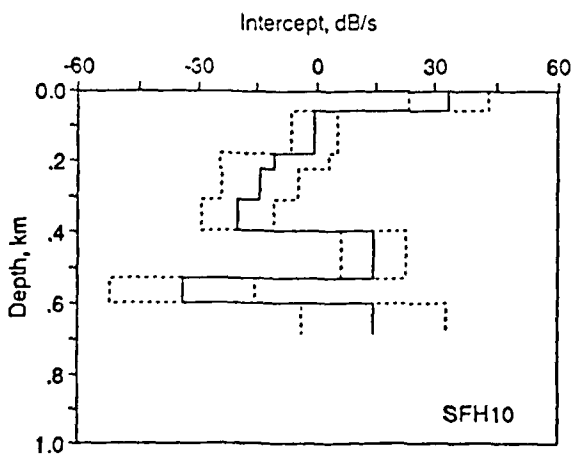
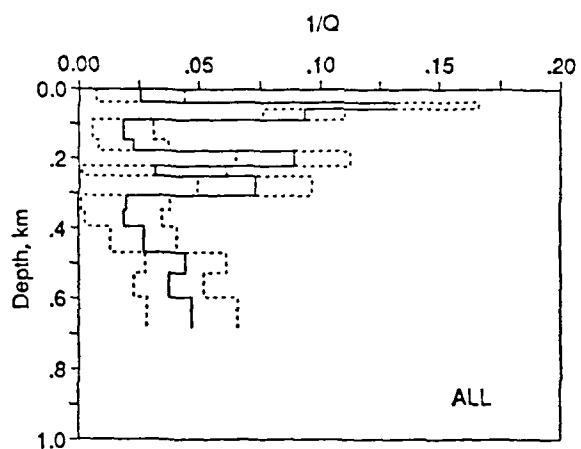
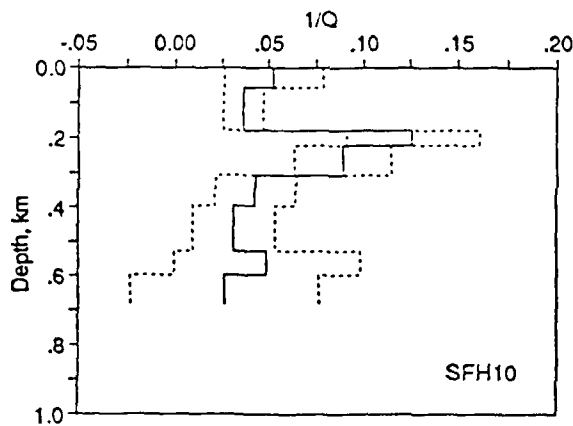


Fig. 7d. Same as Figure 7a, except using only the data from SFH10.

Fig. 7e. Same as Figure 7a, except using all of the data from the receivers.

the oceanic crust. Their results indicate Q between 8 and 100 at ultrasonic frequencies, depending upon the state of alteration and porosity.

There are no direct determinations of values of compressional wave Q for oceanic crust in the literature that we are aware of. Based upon the synthetic seismogram results of others, we can ask whether our results are anomalous or typical for the whole oceanic crust. To answer this question, we will assume a constant value of Q for the entire oceanic crust and apply equation (1) to a typical seismic refraction experiment using near-surface sources and receivers. We will examine the signal to noise ratio for refracted arrivals turning horizontally within layer 3 at a range where caustics and retrograde branches are unimportant. Three shot sizes (13.6, 29.1, and 58.2 kg or 30, 64, and 128 pounds, respectively) will be modeled as detonating at quarter wavelength depths [Shor, 1963] as will receiver depths, to maximize the constructive interference of sea surface reflections. The crustal velocity profile used will be that of Fanfare 4, as reported by Spudich and Orcutt [1980b], modified to eliminate the thin sedimentary cover. Spreading losses and transmission losses were calculated for a range of 32.48 km and a slowness of $0.14613 \text{ s km}^{-1}$. Ambient noise levels were extracted from Urick [1986]. The results, assuming a Q_0 of 50 are shown in Figure 9a. No energy beyond 8 Hz can be received due to the ambient noise levels. Maximum signal to noise ratios (SNR) vary between 11 and 22 dB, depending upon shot size and frequency. These SNR values are consistent with the practices used in two-ship or sonobuoy

experiments where the dynamic range of the recording systems is typically limited to about 20 dB.

Figure 9b shows the effect of changing Q while keeping the shot weight constant at 29.1 kg (64 pounds). Q of 20 for the whole crust would prohibit any recovery of refracted energy. Q of 450 would exhibit some refracted energy beyond 20 Hz. Little if any energy was ever seen at these ranges (G. G. Shor, Jr., personal communication, 1989), although some air gun profiles have likely exhibited higher frequency refracted arrivals. A Q of 450 would also yield SNR values close to 35 dB which would be within the range of recorded levels using multiple recording gains.

Based upon the results of Figure 9, it is probably safe to say that our attenuation results are close to being typical for the whole oceanic crust, although the lower crust may have lower values of attenuation. Further experiments are required to better place our results in an overall picture of crustal attenuation values.

Our attenuation results (Figure 7) do not show any systematic variation with depth, a disappointing result for those interested in correlating attenuation with geologic stratigraphy. The data set used lies entirely within layer 2, the extrusive basalt complex. Neither the attenuation nor velocity profiles show any sublayering within the first 650 m of oceanic crust at this site.

The solutions of attenuation do indicate the possibility of a large excess of frequency-independent attenuation within the first 100 m (Figures 7b and 7d). This may be a real result, due to scattered attenuation caused by the rough seafloor topography or shallow

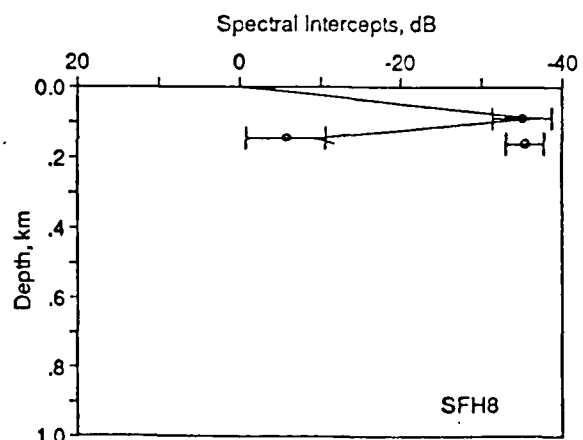
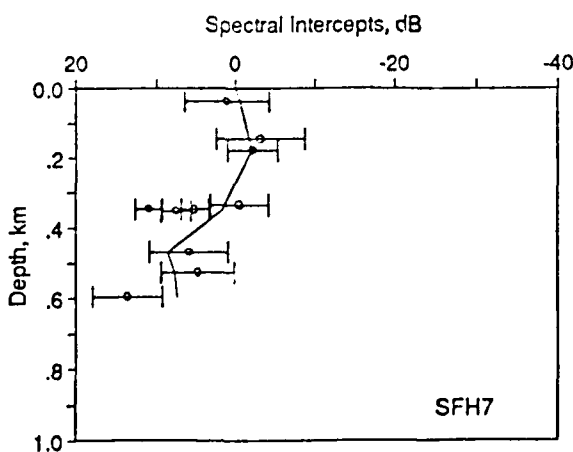
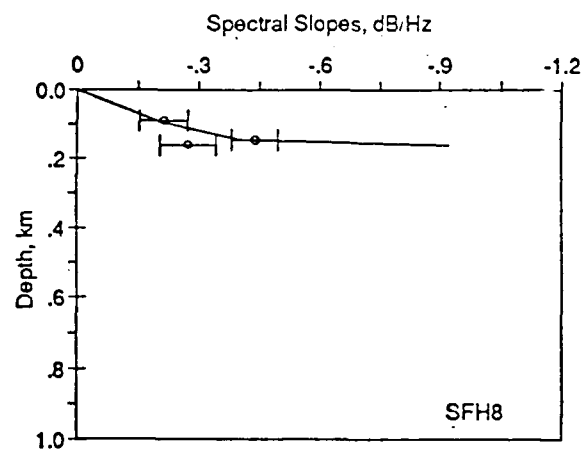
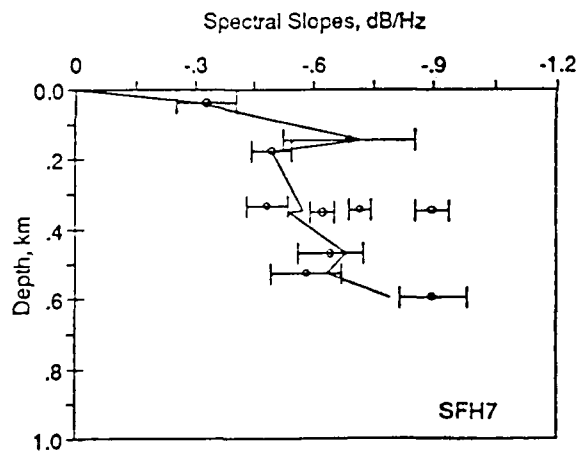


Fig. 8a. Fit of the attenuation versus depth solution shown in Figure 7 to the spectral data of SFH7. See Figure 6a for more information. The predicted curves of spectral slope and attenuation are only approximately correct between data points and interpolation should be avoided.

Fig. 8b. Same as Figure 8a, except using only the data from SFH8.

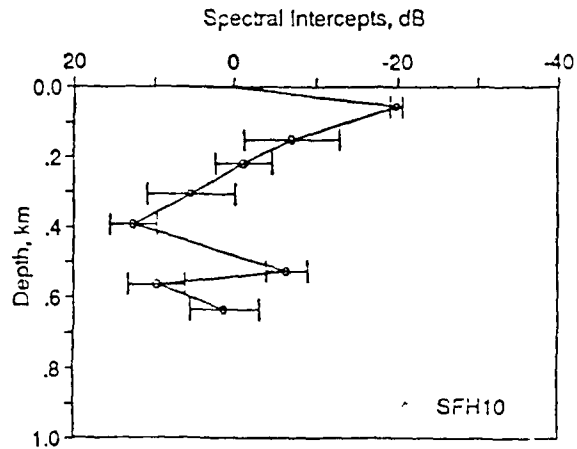
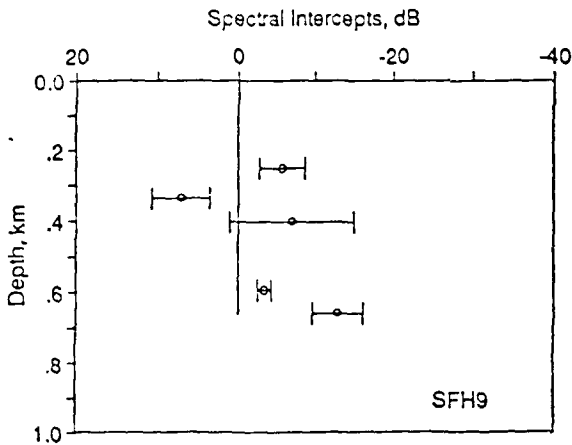
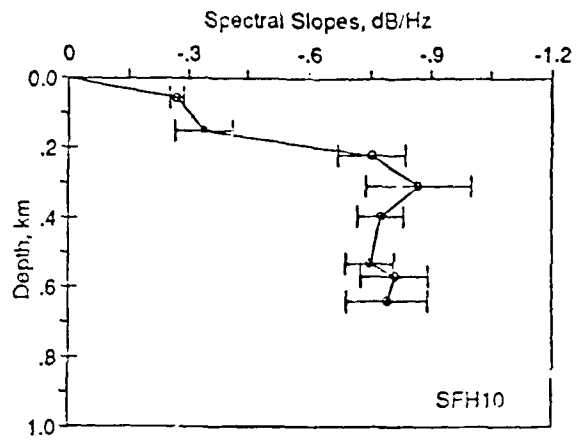
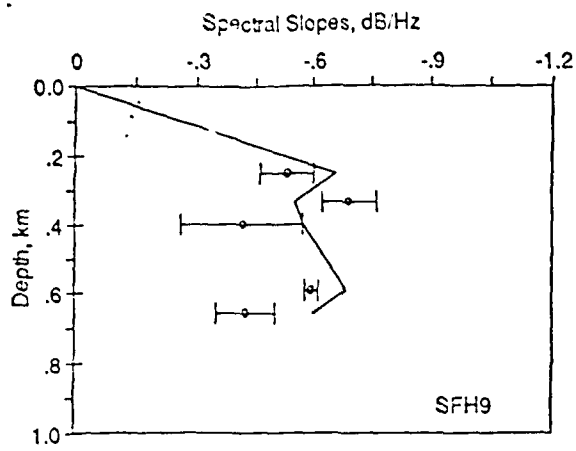


Fig. 8c. Same as Figure 8a, except using only the data from SFH9.

Fig. 8d. Same as Figure 8a, except using only the data from SFH10. In this case, all eigenvalues and eigenvectors (see text for details) were retained, so that the fit to the slope and intercepts are exact.

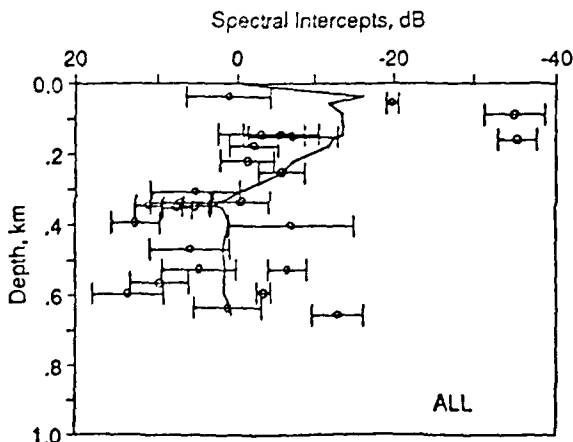
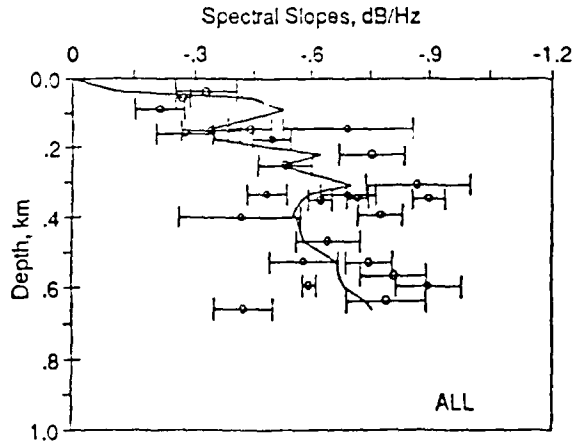


Fig. 8e. Same as Figure 8a, except using all of the data from the receivers.

layering/heterogeneities. This interpretation is reinforced by noting that both SFH8 and SFH10 data sets exhibit this anomalous attenuation, and both receivers are located close to one another (Figure 1). *Poujol and Jacobson [1988]* reported anomalous travel time arrivals for SFH8, suggesting crustal heterogeneities in the immediate vicinity of the receiver.

An alternative explanation for the anomalous frequency-independent attenuation within the first 100 m may be due to inappropriate spreading loss calculations, based upon the velocity depth function. The τ - ζ method of *Dorman and Jacobson [1981]* produces overly smooth velocity depth profiles, due to the averaging of the travel time curve by a low-order polynomial. The spreading loss term (equation (10)) can be simplified for a constant velocity gradient layer. Since

$$x = \frac{2\cos\theta}{p} \frac{dV}{dz} \quad \text{and} \quad \cos\theta = \left(1 - p^2 V_0^2\right)^{1/2} \quad (15)$$

where V_0 is the velocity at the top and p^{-1} is the velocity at the bottom of the layer. Solving for the partial derivative of x with respect to slowness yields

$$\frac{\partial x}{\partial p} = \frac{-1}{x \left(\frac{dV}{dz}\right)^2 p^3} \quad (16)$$

so that the spreading loss term becomes

$$G(x) = \frac{2\cos(\theta)}{V_0 p^2 \left(\frac{dV}{dz}\right)} \quad (17)$$

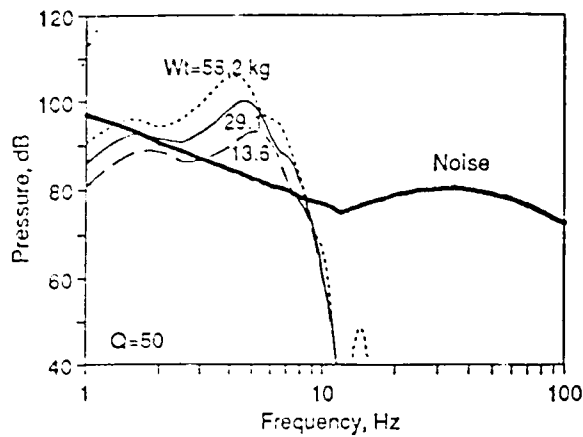


Fig. 9a. Plot of the expected received seismic pressure in dB re $1 \mu\text{Pa Hz}^{-1/2}$ of a layer 3 arrival and ambient noise levels as a function of frequency for a typical two-ship seismic refraction experiment. The range is 32 km, using the velocity depth function of Fanfare 4 [Spudich and Orcutt, 1980b]. The received energy levels differ according to shot size: 13.6 kg (30 pounds, dashed), 29.1 kg (64 pounds, solid) and 53.2 kg (123 pounds, dotted) of TNT. All of the curves assume a Q of 50 for the entire oceanic crust. See text for more details.

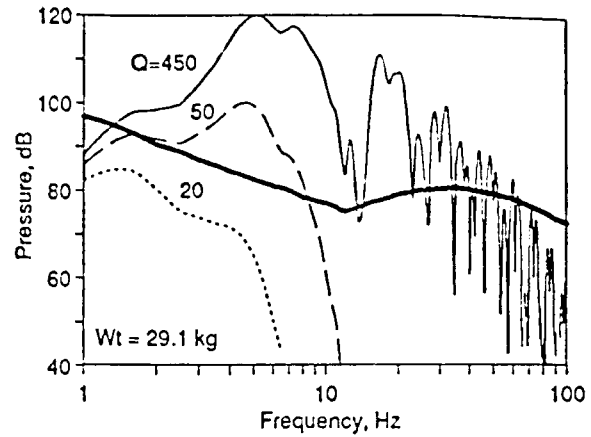


Fig. 9b. Same as Figure 9a, except the charge size was fixed at 29.1 kg (64 pounds) and attenuation was varied: Q equals 20 (dotted), 50 (dashed) and 450 (solid); the latter value is normally assumed for oceanic crust. In all cases, little energy can be recorded above 20 Hz, in accord with observations over the past three decades [Shor, 1963]. While values for Q of 20 are unlikely for the whole oceanic crust, our results of Q between 20 and 50 are largely compatible with values expected for the oceanic crust.

To increase the spreading loss $G(x)$ at shallow depths, one must decrease the velocity gradients, dV/dz , to account for the excess attenuation. It is possible, therefore, to have a more uniform-like shallow layer, assuming that there is only intrinsic attenuation. In the same vein, the deficit of attenuation at depth (Figures 8a and 8d) implies that we have underestimated the velocity gradients.

Our results also demonstrate circumstantial evidence for crustal heterogeneities within the 3-km-wide array. Every attempt to model the data statistically requires a separate solution for each receiver. Some of the models also required a nonphysical 1θ dependence of attenuation. Anomalous travel time residuals and arrivals have also been noted by Poujol and Jacobson [1988]. Tomographic inversion of attenuation would be the logical next step, but the paucity of data and the few overlapping paths would render this exercise futile.

Examination of the data for azimuthal variations, possibly due to aligned vertical cracks, showed no significant correlation. It must be pointed out, however, that our data set is heavily biased towards ray paths in a north-south orientation, due to the position of the receivers relative to the shots (Figure 1). Refracted arrivals from the west and east were observed, but the shot points were located outside the array and thus too poorly located to be useful [Poujol and Jacobson, 1988]. A qualitative comparison of an arrival at SFH3 from the east and from the south at approximately the same range (Figure 10) show a clear amplitude difference. Thus azimuthal variation of attenuation within the shallow crust cannot be ruled out entirely.

Finally, Lewis and Jung [1989] examined a midwater towed array data set using surface charges in the same area as our experiment. Their forward modeling of attenuation indicates that a minimum of attenuation exists at 10 Hz due to the presence of high-velocity gradients in the uppermost crust, which acts to duct high-frequency energy within the high gradient zone. They modeled the attenuation structure with two layers: a 1 km thick upper layer with a Q of 50 overlying a Q half-space of 2000. By fitting their data from 2 to 28 Hz, they found a satisfactory fit, but required a frequency-dependent total Q due to the velocity structure effects. Our data here cannot be used to confirm or refute these conclusions, as our frequency resolution is too poor at low frequencies. Our solutions do not

require frequency-dependent Q to satisfy the data. Further, Lewis and Jung [1989] conclude that the combined effects of the shallow highly attenuating layer and velocity structure limit standard seismic refraction data to be below 30 Hz. The modeling presented here (Figure 9) requires only that path-averaged Q of the crust be less than about 100 to limit the frequency content of typical seismic refraction data.

CONCLUSIONS

The results of the first determination of compressional wave attenuation in the uppermost oceanic crust revealed that attenuation can largely be described by a linear frequency dependence of attenuation and a frequency-independent component of attenuation. Values of Q vary between 20 and 50 for the uppermost 650 m of the crust. The attenuation is significantly higher than those found by modeling data with synthetic seismograms but is in general agreement with recent laboratory data [Wepfer and Christensen, 1987,

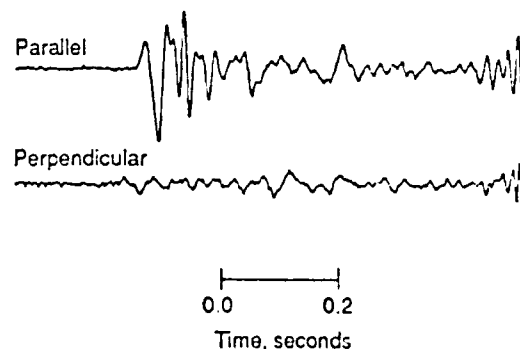


Fig. 10. Equal amplitude plots of shots recorded by SFH8 oriented parallel and perpendicular to the ridge crest at about 2 km range. The shot perpendicular to the ridge crest lies outside the receiving array and could not be adequately located for inclusion in the data inversion. The disparity in amplitudes suggests an azimuthal variation in attenuation, possibly due to vertically oriented cracks and fissures aligned parallel to the ridge crest. A test of the data revealed no azimuthal variation, largely due to the paucity of shots oriented perpendicular to the ridge crest.

this issue]. Based upon modeling of typical seismic refraction data using the sonar equation, the results indicate that our values may be typical to higher than normal values of attenuation for oceanic crust. It is unlikely, however, that values of Q of 20 are present throughout the whole crust.

Our data do not correspond to any fine-scale geological interpretation of the uppermost crust, but this may be a result of an overly smooth velocity depth function, which affects the attenuation models. Our data do indicate a degree of heterogeneity within the oceanic crust. The magnitudes and scales of such heterogeneities cannot be determined, but the spatial scales are likely to be of the order of hundreds of meters. No azimuthal variation of attenuation was evident, although the data set is somewhat inadequate to conclude this result.

Further experiments and results will be necessary to determine whether our results are typical or anomalous for young, upper oceanic crust. Until such time, however, a healthy caution to using the values of Q determined from synthetic seismograms is warranted.

Acknowledgments. We appreciate the efforts of all those who helped collect this data, particularly the Master of the R/V *Wecoma*, Ken Palfrey and the rest of the crew. Special thanks are extended to Paul O'Neill and Tom Fairbanks, who helped prepare the seafloor hydrophones. Michel Poujol helped prepare the seismic data and transcribe it for us as one of us (R.S.J.) made the transition from Oregon State University to the Office of Naval Research. Special thanks go to Dale Bibee, who provided codes to calculate shot spectra. Ellen Kappel kindly provided the regional map of the Juan de Fuca region. This paper was reviewed by R. Stephen and an anonymous reviewer, both of whom provided excellent guidance for revisions. This work was performed under ONR contract N00014-84C-0218 while R.S.J. was at OSU and under ONR contract N00014-89WX24098 while at ONR. B.T.R.L. was funded under ONR contract N00014-84-C-0111.

REFERENCES

- Aki, K., and P. G. Richards, *Quantitative Seismology*, 932 pp., W. H. Freeman, New York, 1980.
- Collins, J. A., G. M. Purdy, and T. M. Brocher, Seismic velocity structure at Deep Sea Drilling Project site 504B, Panama Basin: Evidence for thin crust, *J. Geophys. Res.*, **94**, 9283-9302, 1989.
- Dorman, L. M., and R. S. Jacobson, Linear inversion of body wave data, I. Velocity structure from travel times and ranges, *Geophysics*, **46**, 138-151, 1981.
- Ewing, J. I., and G. M. Purdy, Upper crustal velocity structure in the ROSE area of the East Pacific Rise, *J. Geophys. Res.*, **87**, 8397-8402, 1982.
- Harding, A. J., J. A. Orcutt, M. E. Kappus, E. E. Vera, J. C. Mutter, P. Buhl, R. S. Detrick, and T. M. Brocher, Structure of young oceanic crust at 13°N on the East Pacific Rise from expanding spread profiles, *J. Geophys. Res.*, **94**, 12,163-12,196, 1989.
- Jacobson, R. S., An investigation into the fundamental relationships between attenuation, phase dispersion and frequency using seismic refraction profiles over sedimentary structures, *Geophysics*, **52**, 72-87, 1987.
- Jacobson, R. S., G. G. Shor, Jr., and L. M. Dorman, Linear inversion of body wave data, II, Attenuation versus depth using spectral ratios, *Geophysics*, **46**, 152-162, 1981.
- Jacobson, R. S., G. G. Shor, Jr., and M. Bèe, A comparison of velocity and attenuation between the Nicobar and Bengal Deep Sea Fans, *J. Geophys. Res.*, **89**, 6181-6196, 1984.
- Johnson, R. V., II, C. R. B. Lister, and B. T. R. Lewis, A direct recording ocean bottom seismometer, *Mar. Geophys. Res.*, **3**, 65-85, 1977.
- Johnston, D. H., and M. N. Toksöz, Definitions and terminology, in *Seismic Wave Attenuation*, edited by M. N. Toksöz and D. H. Johnston, pp. 1-5, Society of Exploration Geophysics, Tulsa, Okla., 1981.
- Jung, H., Velocity and attenuation in young ocean crust, Ph.D. thesis, 124 pp., Univ. of Wash., Seattle, May 1988.
- Kjartansson, E., Constant Q -wave propagation and attenuation, *J. Geophys. Res.*, **84**, 4737-4748, 1979.
- Lewis, B. T. R., and H. Jung, Attenuation of seismic waves in the upper oceanic crust (abstract), *Earthquake Notes*, **55**, 24, 1984.
- Lewis, B. T. R., and H. Jung, Attenuation of refracted seismic waves in young ocean crust, *Bull. Seismol. Soc. Am.*, **79**, 1070-1088, 1989.
- Little, S. A., and R. A. Stephen, Costa Rica rift borehole seismic experiment, *Initial Rep. Deep Sea Drill. Proj.*, **83**, 517-528, 1985.
- Naval Ordnance System Command, NAVORD OP3696, Technical Manual, Explosives safety precaution for research vessels, Washington, D.C., 1973.
- Osle, B., and R. W. Mensing, *Statistics in Research*, 596 pp., Iowa State University Press, Ames, 1975.
- Poujol, M., and R. S. Jacobson, Using inverse theory and Seabeam bathymetry to improve seismic refraction data corrections, *Mar. Geophys. Res.*, **9**, 311-332, 1988.
- Purdy, G. M., The correction for the travel time effects of seafloor topography in the interpretation of marine seismic data, *J. Geophys. Res.*, **87**, 8389-8396, 1982.
- Purdy, G. M., A determination of the seismic velocity structure of sediments using both sources and receiver near the ocean floor, *Mar. Geophys. Res.*, **8**, 75-91, 1986.
- Purdy, G. M., New observations of the shallow seismic structure of young oceanic crust, *J. Geophys. Res.*, **92**, 9351-9362, 1987.
- Sauter, A. W., L. M. Dorman, and A. E. Schreiner, A study of sea floor structure using ocean bottom shots and receivers, in *Ocean Seismo-Acoustics*, edited by T. Akal and J. M. Berkson, pp. 673-682, Plenum, New York, 1986.
- Shor, G. G., Jr., Refraction and reflection techniques and procedures, in *The Sea*, vol. 3, edited by M. N. Hill, pp. 20-38, Wiley-Interscience, New York, 1963.
- Shor, G. G., Jr., Cruise report, Mariana Leg 10, *SIO Ref. 79-8*, Scripps Inst. of Oceanogr., La Jolla, Calif., 1979.
- Spudich, P., and J. Orcutt, A new look at the seismic velocity structure of the oceanic crust, *Rev. Geophys.*, **18**, 627-645, 1980a.
- Spudich, P., and J. Orcutt, Petrology and porosity of an oceanic crustal site: Results from waveform modeling of seismic refraction data, *J. Geophys. Res.*, **85**, 1409-1433, 1980b.
- Stephen, R. A., Lateral heterogeneity in the upper oceanic crust at Deep Sea Drilling Project site 504, *J. Geophys. Res.*, **93**, 6571-6584, 1988.
- Stephen, R. A., and A. J. Harding, Travel time analysis of borehole seismic data, *J. Geophys. Res.*, **88**, 8289-8298, 1983.
- Stephen, R. A., K. E. Loudon, and D. H. Matthews, The oblique seismic experiment on DSDP leg 52, *Geophys. J. R. Astron. Soc.*, **60**, 289-300, 1980.
- Swift, S. A., and R. A. Stephen, Lateral heterogeneity in the seismic structure of the upper oceanic crust, western North Atlantic, *J. Geophys. Res.*, **94**, 9303-9322, 1989.
- Urick, R. J., *Ambient Noise in the Sea*, Peninsula Publishing, Los Altos, Calif., 1986.
- Vera, E. E., Seismic structure of 0- to 4.5 MY-old oceanic crust between 9°N and 13°N on the East Pacific Rise, Ph.D. thesis, 127 pp., Columbia Univ., New York, March 1989.
- Wepfer, W. W., and N. I. Christensen, Characterizing microcracks via a velocity-pressure relation (abstract), *Eos, Trans. AGU*, **58**, 1503, 1987.
- Wepfer, W. W., and N. I. Christensen, Compressional wave attenuation in oceanic basalt, *J. Geophys. Res.*, this issue.
- Wiggins, R. A., The general linear inverse problem: Implications of surface waves and free oscillations for earth structure, *Rev. Geophys.*, **10**, 251-285, 1972.

R. S. Jacobson, Office of Naval Research, Marine Geology and Geophysics, Code 1125GG, Arlington, VA 22217

B. T. R. Lewis, School of Oceanography, University of Washington, Seattle, WA 98195

(Received September 1, 1989;
revised January 9, 1990;
accepted March 22, 1990.)